

See discussions, stats, and author profiles for this publication at: <http://www.researchgate.net/publication/267638838>

Marangoni ring-templated vertically aligned ZnO nanotube arrays with enhanced photocatalytic hydrogen production

ARTICLE *in* MATERIALS CHEMISTRY AND PHYSICS · JANUARY 2015

Impact Factor: 2.26 · DOI: 10.1016/j.matchemphys.2014.10.046

CITATIONS

3

READS

83

10 AUTHORS, INCLUDING:



[Wei Cheat Lee](#)

University of Sussex

5 PUBLICATIONS 3 CITATIONS

SEE PROFILE



[Giacomo Edi Canciani](#)

University of Sussex

5 PUBLICATIONS 3 CITATIONS

SEE PROFILE



[Sulaiman Mohammed Alfadul](#)

King Abdulaziz City for Science and Techno...

28 PUBLICATIONS 50 CITATIONS

SEE PROFILE

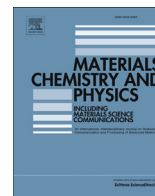


[Christopher C Perry](#)

Loma Linda University

52 PUBLICATIONS 646 CITATIONS

SEE PROFILE



Materials science communication

Marangoni ring-templated vertically aligned ZnO nanotube arrays with enhanced photocatalytic hydrogen production



Wei Cheat Lee^a, Yuanxing Fang^a, Rantej Kler^a, Giacomo E. Canciani^a, Thomas C. Draper^a, Zainab T.Y. Al-Abdullah^a, Sulaiman M. Alfadul^b, Christopher C. Perry^c, Heyong He^d, Qiao Chen^{a,*}

^a Chemistry Department, School of Life Sciences, Sussex University, Brighton BN1 9QJ, UK

^b King Abdulaziz City for Science and Technology, P.O. Box 6086, Riyadh 11442, Saudi Arabia

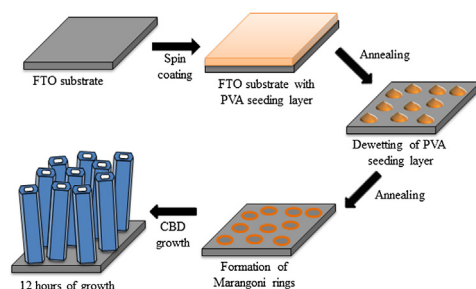
^c Biochemistry Division, School of Medicine, Loma Linda University, Loma Linda, CA 92350, USA

^d Chemistry Department and Shanghai Key Laboratory of Molecular Catalysis and Innovative Materials, Fudan University, Shanghai 200433, PR China

HIGHLIGHTS

- First time using Marangoni ring-structured template for synthesising ZnO NTs.
- Ring structures are formed with the presence of PVA in the seeding solution.
- The PEC water splitting of ZnO NTs is three times more efficient than NRs.
- 0.45% of AM1.5G efficiency and 9% UV efficiency were achieved by ZnO NTs.

GRAPHICAL ABSTRACT



ARTICLE INFO

Article history:

Received 24 July 2014

Received in revised form

1 October 2014

Accepted 26 October 2014

Available online 2 November 2014

Keywords:

Nanotube arrays
Marangoni mechanism
Chemical bath deposition
Hydrogen generation

ABSTRACT

Here we report on a novel approach for the synthesis of vertically aligned hexagonal ZnO nanotube arrays. Ring-like structures were formed on substrate using the polymer-based seeding solution through the Marangoni mechanism, guiding the growth of ZnO nanotubes with aqueous chemical bath deposition. Photoelectrochemical hydrogen generation by water splitting on a ZnO nanotube anode is about three times as efficient as that on a similar ZnO nanorod anode.

© 2014 Elsevier B.V. All rights reserved.

1. Introduction

Direct harvesting of solar energy by photoelectrochemical (PEC) hydrogen generation offers a novel renewable energy source. Since TiO₂ was first reported for PEC water splitting in 1972 [1], many

one-dimensional semiconductor nanostructures (e.g. ZnO [2], SnO₂ [3], GaN [4] and Fe₂O₃ [5]), including nanorods (NRs) [6], nanotubes (NTs) [7] and nanowires [6], have been designed for improving the solar energy harvesting efficiency.

Wide band gap metal oxide nanotubular structures with large surface areas, excellent electrolyte transportation and good electrical contact with substrates e.g. vertically aligned TiO₂ NTs [7], have attracted extensive investigation for their potential

* Corresponding author.

E-mail address: qiao.chen@sussex.ac.uk (Q. Chen).

applications in PEC water splitting [8]. Other than TiO_2 , ZnO has received great attention due to the wide direct band gap and have shown promising potential as a photocatalyst [3]. Recently, vertically aligned ZnO NRs have been shown to have potential applications in photovoltaic [9] and photocatalytic water splitting [2]. However, the exploitation of vertically aligned ZnO NTs is still very limited [10–13], due to the lack of reproducible controlled synthesis.

In this communication, we report a new bottom-up direct synthesis of vertically aligned crystalline ZnO nanotubular structures from a ring-patterned template, made through the Marangoni mechanism [14]. PEC measurements reveal that NT anodes are roughly three times more efficient than their NR counterparts.

2. Materials and methods

All the chemicals used were analytical grade and purchased from Sigma–Aldrich. Fluorine-doped tin oxide (FTO) glasses (4 cm^2) were sonicated in an isopropanol (IPA) bath for 15 min and dried in air before coating a seeding layer. Different seeding solutions were used for growing ZnO NRs and NTs. For ZnO NRs, 2.19 g of zinc acetate in 10.0 mL of DI water was stirred for 2 h to give a 1.0 M seeding solution. For ZnO NTs, the seeding solution had the same concentration of zinc acetate with the addition of 0.60 g of polyvinyl alcohol (PVA, MW ~25,000, 88% hydrolysed) in the 10.0 mL solution. The seeding solutions were spin coated on the substrates at different spin speed in order to compensate the difference in viscosity. The coating of the NR seeding solution (without PVA) was made at lower spin speed (300 rpm), in comparison to 800 rpm for the coating of the NT seeding solution (with PVA).

The coated samples were then heated in air at a constant heating rate of $10 \text{ }^\circ\text{C}/\text{min}$ to $350 \text{ }^\circ\text{C}$. This temperature was held for one hour to remove PVA and to convert the zinc acetate into ZnO nanocrystal seeds. Vertically aligned ZnO NTs were grown via the chemical bath deposition (CBD) method in a nutrient solution consisting of a 1:1 molar ratio of zinc nitrate hexahydrate (0.59 g) and hexamethylenetetramine (HMT; 0.28 g) in 200 mL DI water. The final concentration of Zn^{2+} in the growth solution was 10.0 mM. The seeded FTO glasses were placed in 100 mL of growth solution for 12 h at $85 \text{ }^\circ\text{C}$. The samples were allowed to cool to room temperature, rinsed with DI water and air dried.

Step-wise temperature-dependent attenuated total reflectance–Fourier transform infrared spectroscopy (ATR–FTIR, Perkin Elmer Spectrum One) measurements were carried out to monitor the PVA decomposition process of the seeding layer. The surface morphologies were studied by scanning electron microscopy (SEM, JSM 820M, Jeol). The crystallinity and structure orientation of the nanostructures were analysed by powder x-ray diffraction (XRD, Siemens D500). The UV–visible absorption spectra were recorded using UV–visible spectrophotometer (Thermospectronic UV 300). The average diameters and average film thicknesses were measured from top- and side-view SEM images using Image J (NIH, USA). The PEC water splitting was measured using a standard three-electrode configuration in a 1.0 M KOH electrolyte. A platinum foil was used as counter electrode and a KCl saturated Ag/AgCl electrode was used as a reference. A USB potentiostat (eDAQ) was used to control and record the photocurrent as a function of electrochemical potential. Sunlight was simulated with a 300W xenon arc lamp with an AM1.5G filter and the output light power density was adjusted to 100 mW cm^{-2} . The optical power density was calibrated by a power metre (Newport 1830-C) with a wide band sensor (Newport 818-UV attenuated).

3. Results and discussion

Ring-like structures were formed in the seeded layer with PVA (Fig. 1A), without PVA, only cubic crystalline ZnO seeds were formed (Fig. 1B). The ring formation may be explained by the convective evaporation–decomposition. When annealing, the PVA film began to melt and formed drops due to the dewetting before decomposition. The dome profile causes a temperature gradient from the centre to the edge of droplet leading to the decomposition of PVA at the circular edge [15]. The liquid removed from the edge is replenished by an outward flow of molten PVA and zinc acetate, at a slowly increasing temperature [14]. The optimal conditions for the rings formation were with heating at a constant rate of $10 \text{ }^\circ\text{C}/\text{min}$ to $350 \text{ }^\circ\text{C}$. With a lower temperature of $300 \text{ }^\circ\text{C}$, only a small number of rings were formed (Fig. 1C). If the heating rate was too rapid ($15 \text{ }^\circ\text{C}/\text{min}$), webs, instead of rings, were formed (Fig. 1D), suggesting that PVA evaporation rate was faster than the inflow of the molten polymer. The temperature dependent ATR–FTIR measurement revealed that at $350 \text{ }^\circ\text{C}$, PVA was fully decomposed, meanwhile the zinc acetate was converted to ZnO (see temperature dependent ATR–FTIR data in Fig. S1, Supporting Information).

Fig. 1E and F shows vertically aligned NTs with mean length of $5.0 \text{ }\mu\text{m}$, mean outer diameter of $159 \pm 36 \text{ nm}$ and mean wall thickness of $41 \pm 12 \text{ nm}$ were formed after 12 h. The average distance between the centres of the adjacent NTs is $\sim 180 \text{ nm}$. The mean dimensions and their errors were evaluated from 100 measurements. Without PVA in the seeding solution, vertically aligned crystalline ZnO NRs were formed (Fig. 1F and H). The dimensions of the NRs were very similar to those of the NTs, where its mean diameter was $157 \pm 30 \text{ nm}$ with a mean length of $4.5 \text{ }\mu\text{m}$.

The XRD patterns (Fig. 2) of hexagonal ZnO NTs and NRs were compared with the wurtzite ZnO (JCPDS 36-1451) standard. The diffraction pattern from ZnO powder was also included as a reference. In comparison with the ZnO powder, the (002) peak is dominant for the NRs. This is contributed from the vertical orientation of NRs with their (002) planes parallel to the substrate. However, NTs display a much lower (002) peak intensity due to the reduced scattering from the (002) plane at the tube centre. Quantitative analysis of the diffraction intensities reveals that the intensity ratios of the ZnO powder are 1.0:0.7:1.5 for (100):(002):(101) planes. This ratio changes to 1.0:1.0:1.2 for ZnO NTs. This analysis suggests that the NTs are possibly aligned perpendicular to the substrate. Crystal sizes in the NTs were determined from the Scherrer equation [16]. Larger single crystal domains were observed for the (100) and (101) planes (26.4 nm and 30.4 nm), than for the (002) plane (21.2 nm) in NTs, restricted by the wall thickness.

The UV–visible absorption was used to measure the band gaps of the nanostructures, using the Tauc equation from the extinction coefficient (α) as a function of photon energy ($h\nu$) [17]. The absorption spectra together with the plot of $(\alpha h\nu)^2$ vs $h\nu$ are shown in Fig. 3. The linear nature of the Tauc plots at the absorption edge confirms that the films are semiconductors with direct band gaps. The red shift of NT indicates that the NTs have a smaller optical band gap (3.13 eV) than the NRs (3.21 eV). The smaller band gap is attributed to small crystal domain size and wall thickness of the NTs.

The PEC performance of the NT and NR samples grown under identical conditions for 12 h was compared. Fig. 4A shows the current–voltage curves for NT and NR photoanodes in darkness, light on–off and under simulated sunlight between potentials of -0.4 and $1.0 \text{ V}_{\text{Ag}/\text{AgCl}}$. When illuminated, the photocurrent from both ZnO NT and NR anodes increase steeply at lower potential with onset at $-0.36 \text{ V}_{\text{Ag}/\text{AgCl}}$ for NT and $-0.38 \text{ V}_{\text{Ag}/\text{AgCl}}$ for NR. The onset potential is approximately equal to the conduction band edge

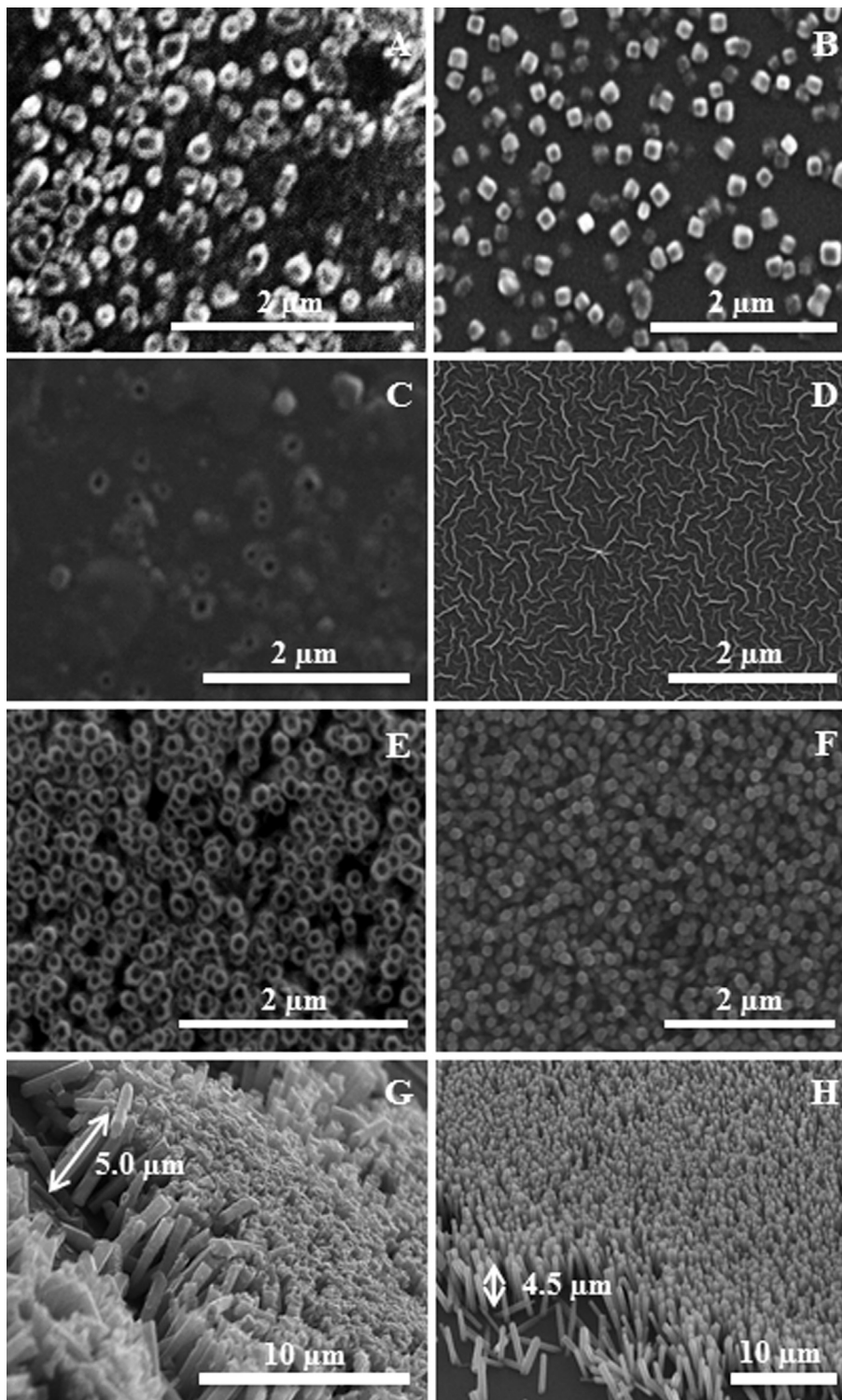


Fig. 1. SEM images of seed layer with PVA (A) and without PVA (B). SEM images of seed layer with PVA at 300 °C (10 °C/min) (C) and 350 °C (15 °C/min) (D). SEM top view and titled view of ZnO NTs (E,G) and ZnO NRs, respectively (F,H).

potential (E_c). Toward the positive potential, the photocurrent density generated from the NTs increases much faster than the NRs. Measured at 0.0 $V_{Ag/AgCl}$, the NTs generate 0.49 mA cm^{-2} , while NRs generate only 0.17 mA cm^{-2} . The light on–off spectrum confirms that the current was generated by the photoexcitation. For both samples, the photocurrent increase slows down at potentials

higher than 0.08 $V_{Ag/AgCl}$, but does not plateau. This suggests that charge recombination and interface reaction kinetics did not limit the photocurrent under our experimental conditions. Amperometric studies were carried out for both the NT and NR photoanodes at an applied voltage of 0.2 $V_{Ag/AgCl}$ under light on–off cycles for 600 s. There is no obvious decrease in the photocurrents, which

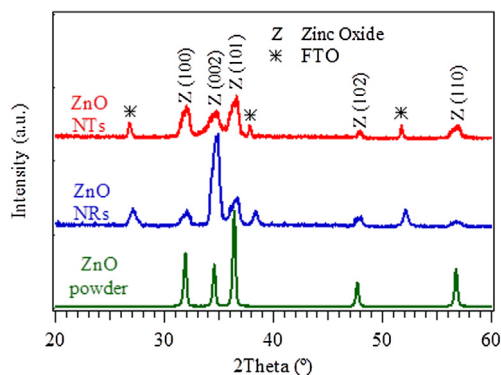


Fig. 2. Surface XRD spectra of ZnO NTs and NRs on FTO glasses with a film thickness of ~5 μm in comparison with ZnO powder.

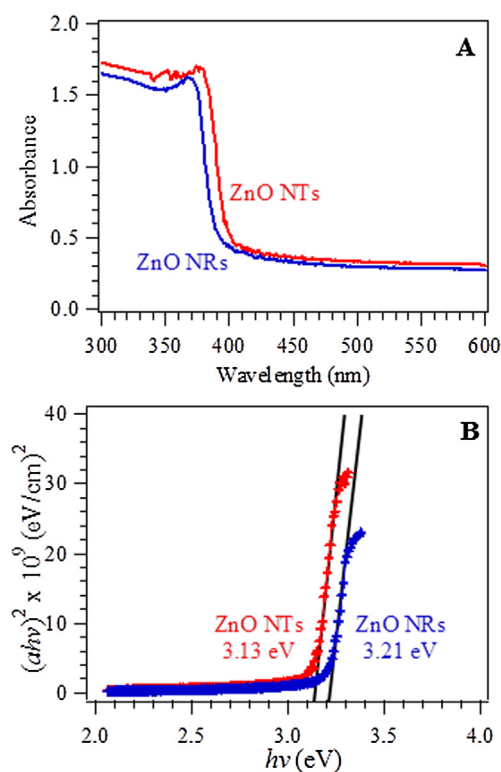


Fig. 3. (A) UV–visible absorption spectra and (B) Tauc plots of ZnO NTs and NRs.

confirms that both the NTs and NRs are stable under our experimental conditions (see *I*-*t* curves in Fig. S2, Supporting Information).

Solar-conversion efficiencies (η) formulated as $\eta(\%) = J_p [E_{\text{rev}} - E_{\text{app}} / I_0] * 100$ [18], were shown in Fig. 4B. J_p is the photocurrent density, $E_{\text{rev}} = 1.23$ V, $E_{\text{app}} = E_{\text{meas}} - E_{\text{oc}}$ where E_{meas} is the working electrode potential (vs. Ag/AgCl) and E_{oc} is the working electrode potential (vs. Ag/AgCl) under open circuit condition ($J_p = 0$ mA cm⁻²) whilst illuminated, and I_0 is the incident light power intensity. As the ZnO NTs and NRs have band gaps larger than 3.1 eV, only the UV part of the light was absorbed. As such, we calculated the photoefficiency against the energy densities from both the UV and the full solar spectrum. Under AM1.5G illumination, NTs anode achieves a higher conversion power than NRs anode, with a maximum output power of 0.45 mW cm⁻², instead of 0.15 mW cm⁻². These correspond to

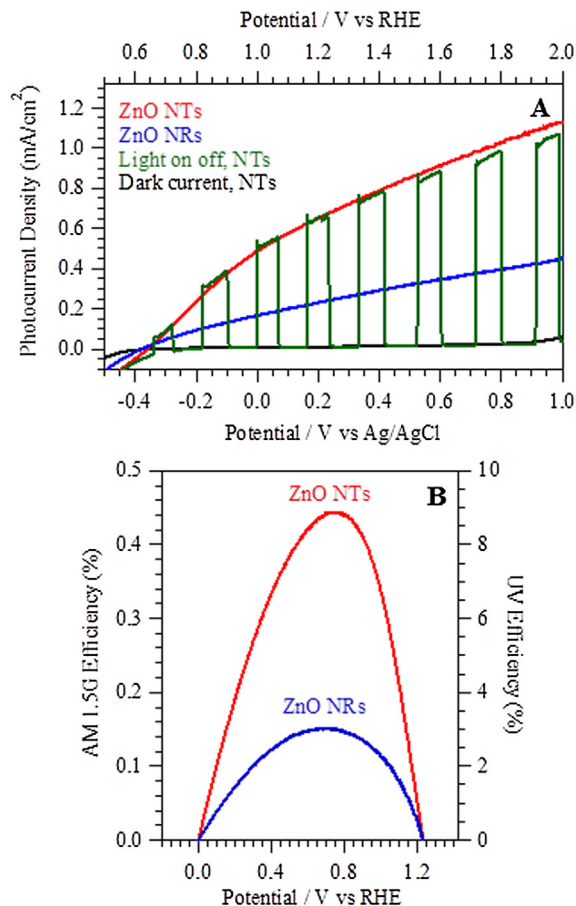


Fig. 4. (A) Photocurrent generated from ZnO NTs and ZnO NRs together with the dark current and light on-off current measured from ZnO NTs and (B) corresponding UV and AM1.5G photoefficiency.

AM1.5G efficiencies of 0.45% (NTs) and 0.15% (NRs) and UV photoefficiencies of 9% (NTs) and 3% (NRs). The photoefficiency of our ZnO NT anode was also compared with the ZnO NTs prepared by electrochemical method [10]. The efficiency of our NTs is three times higher for water splitting, which could be due to their limited tube length and poor orientation.

The main differences between the ZnO NTs and NRs are their morphologies and electronic structures. The surface porosity (P) of the NTs sample is calculated to be 53%, higher than 43% from the NRs [19]. The additional nano-channels from NTs improve the transport of electrolytes and the access of effective surface area for the photocatalytic oxidation. The effective surface area density, quantified as the surface area to volume ratio ($SAVR$), related to the density of available reaction centres for the oxidation of water at the solid–liquid–gas interface. Our measurement reveals that the $SAVR$ of NTs is c.a. 0.027 nm⁻¹, much larger than 0.017 nm⁻¹ of NRs [20], which also contribute to the higher photoefficiency. More importantly, our ZnO NTs have a wall thickness of 41 nm, which is considerably less than the hole diffusion length for crystalline ZnO (~125 nm) [21]. So the electron–hole recombination is expected to be significantly reduced for the NTs, with respect to the NRs [13]. Most importantly, NTs benefit from a smaller band gap, so that intense longer wavelength light can be absorbed. In summary, the combined effects of small band gap, large P , large $SAVR$, and small hole transfer pathway have contributed to the increase of PEC hydrogen generation efficiency of ZnO NTs by three-fold.

4. Conclusions

We have demonstrated, for the first time, direct synthesis of vertically aligned crystalline ZnO NTs from a ring-structured template by the Marangoni mechanism. The PEC measurements reveal that NTs are about three times more efficient than NRs with similar dimensions. Possible mechanisms for the high efficiency are also discussed.

Acknowledgements

W.C. Lee would like to thank Malaysia Public Service Department for his scholarship.

Appendix A. Supplementary data

Supplementary data related to this article can be found at <http://dx.doi.org/10.1016/j.matchemphys.2014.10.046>.

References

- [1] A. Fujishima, K. Honda, *Nature* 238 (1972) 37–38.
- [2] J.W. Miao, H.B. Yang, S.Y. Khoo, B. Liu, *Nanoscale* 5 (2013) 11118–11124.
- [3] T. Nakajima, K. Shinoda, T. Tsuchiya, *Chem. Soc. Rev.* 43 (2014) 2027–2041.
- [4] J. Goldberger, R.R. He, Y.F. Zhang, S.W. Lee, H.Q. Yan, H.J. Choi, P.D. Yang, *Nature* 422 (2003) 599–602.
- [5] T. Lopes, L. Andrade, F. Le Formal, M. Gratzel, K. Sivula, A. Mendes, *Phys. Chem. Chem. Phys.* 16 (2014) 16515–16523.
- [6] S. Barth, F. Hernandez-Ramirez, J.D. Holmes, A. Romano-Rodriguez, *Prog. Mater. Sci.* 55 (2010) 563–627.
- [7] V. Muller, P. Schmuki, *Electrochem. Commun.* 42 (2014) 21–25.
- [8] Z.H. Zhang, P. Wang, *Energy Environ. Sci.* 5 (2012) 6506–6512.
- [9] M.F. Hossain, T. Takahashi, S. Biswas, *Electrochem. Commun.* 11 (2009) 1756–1759.
- [10] Y.K. Hsu, Y.G. Lin, Y.C. Chen, *Electrochem. Commun.* 13 (2011) 1383–1386.
- [11] G.W. She, X.H. Zhang, W.S. Shi, X. Fan, J.C. Chang, *Electrochem. Commun.* 9 (2007) 2784–2788.
- [12] Y.J. Kim, H. Yoo, C.H. Lee, J.B. Park, H. Baek, M. Kim, G.C. Yi, *Adv. Mater.* 24 (2012) 5565–5569.
- [13] N. Chouhan, C.L. Yeh, S.F. Hu, R.S. Liu, W.S. Chang, K.H. Chen, *Chem. Commun.* 47 (2011) 3493–3495.
- [14] R.D. Deegan, O. Bakajin, T.F. Dupont, G. Huber, S.R. Nagel, T.A. Witten, *Nature* 389 (1997) 827–829.
- [15] R.D. Deegan, *Phys. Rev. E* 61 (2000) 475–485.
- [16] A. Weibel, R. Bouchet, F. Boulc'h, P. Knauth, *Chem. Mater.* 17 (2005) 2378–2385.
- [17] A.A. Tahir, M.A. Ehsan, M. Mazhar, K.G.U. Wijayantha, M. Zeller, A.D. Hunter, *Chem. Mater.* 22 (2010) 5084–5092.
- [18] R. Saito, Y. Miseki, K. Sayama, *Chem. Commun.* 48 (2012) 3833–3835.
- [19] $P_{NT} = 1 - (3(w^2 + dw)/l^2)$ and $P_{NR} = 1 - 3D^2/(4l^2)$ where w is the wall thickness, d is the inner diagonal length of NT, D is the diagonal width of the NR and l is the average distance between the centre of adjacent NTs or NRs
- [20] $SAVR_{NT} = (4\sqrt{3} + 3w/T)(d + w)/l^2$ and $SAVR_{NR} = D(2\sqrt{3} + 3D/4T)/l^2$ where w , d , D , l are the same as in ref. 19 and T is the length NTs or NRs
- [21] A. Soudi, P. Dhakal, Y. Gu, *Appl. Phys. Lett.* 96 (2010) 253115.